Saturated absorption spectroscopy of HD at 76 K

Qian-Hao Liu,[1,*] Ya-Nan Lv,[2,*] Chang-Ling Zou,[2] Cun-Feng Cheng,[1,†] and Shui-Ming Hu[1]
[1]*Department of Chemical Physics, University of Science and Technology of China, Hefei 230026, China*
[2]*CAS Key Laboratory of Quantum Information, University of Science and Technology of China, Hefei 230026, China*

(Received 2 May 2022; revised 11 October 2022; accepted 7 November 2022; published 5 December 2022)

Precision spectroscopy of molecular hydrogen can be used to test the quantum electrodynamics theory and determine the proton-to-electron mass ratio in a four-body system. Saturated absorption spectroscopy of the R(1) line in the (2-0) band of HD is measured at 76 K. An asymmetric line profile is observed and analyzed, and the transition frequency is predicted to be 217 105 182 284 $(11)_{\mathrm{stat}}(27)_{\mathrm{sys}}$ kHz. The value is nine times more accurate than our previous result obtained at room temperature and differs by 6.6σ from the recent result derived with a different line-shape model.

DOI: 10.1103/PhysRevA.106.062805

Introduction. The hydrogen molecule is one of the simplest calculable multielectron systems. The comparison between accurate spectroscopy measurements and calculations of H_2 and its isotopologues allows us to test the fundamental interaction theories and determine physical constants [1,2] such as the proton-to-electron mass ratio. The latest theoretical calculation of energy levels of molecular hydrogen takes into account relativistic and high-order quantum electrodynamics (QED) terms, and the fractional accuracy reaches 7×10^{-10} [3,4]. Recent experimental results have been compared with theoretical calculations, leading to an examination of QED corrections in H_2 [5–7] and D_2 [8], the relativistic effect in T_2 [9], and other tritium-bearing isotopologues [10,11], and the nuclear-spin-symmetry conservation between *ortho*- and *para*-H_2 [12].

Although the theoretical treatment for HD is the same as that for H_2 and D_2, there is a much larger (more than 3σ) discrepancy between the experimental and theoretical dissociation energies of HD [4]. Meanwhile, a few terms in the calculation cancel to a large degree for rotation-vibration energies of the hydrogen molecule, leading to a significant reduction in the uncertainty, thereby allowing for accurate QED examinations with infrared transitions. Tests have been performed on infrared transitions among rovibrational levels in H_2 and D_2 with increasing accuracy [13–16]. Because of the presence of weak electronic dipole moments in HD, vibrational transitions of HD are much stronger than those in H_2 and D_2. Various spectroscopy methods have been used in the determination of the rotation-vibration energies of HD. Doppler-broadened infrared absorption spectroscopy in the fundamental and overtone bands has been reported with uncertainties at the level of MHz or sub-MHz [17–19]. Using a molecular beam, Fast and Meek [20] reported the R(0) line in the (1-0) band with an accuracy of 13 kHz, which is so far the best accuracy in the infrared transition of HD, indicating a deviation of 1 MHz from the theoretical result [21]. Cavity-enhanced Lamb-dip spectroscopy of the R(1) line in the (2-0) band has been reported by the Hefei group [22] with cavity ring-down spectroscopy (CRDS) and the Amsterdam group [23] with noise-immune cavity-enhanced optical heterodyne molecular spectroscopy (NICE-OHMS). Both groups declared uncertainties below 0.1 MHz, but there was a discrepancy of 0.9 MHz between the two results, as shown in Fig. 1. Later a line-shape distortion was revealed by the Amsterdam group [24] and also confirmed by the Hefei group [25] with different spectroscopy methods. All the measured results differs from the theoretical result by 2σ.

Here we present a saturated absorption spectroscopy measurement of the R(1) (2-0) line of HD at a temperature of 76 K. The transition frequency is obtained from the line-shape-model analysis based on quantum optical calculations.

Experiments. The low-temperature comb-locked CRDS system is schematically depicted in Fig. 2. The 62.4-cm-long high-finesse (∼130 000) cavity comprises a pair of curved high reflectors, and one of the mirrors is mounted on a piezoelectric actuator (PZT). An oxygen-free high-thermal-conductivity copper cell is contacted to a two-stage cryogenic cooler to produce the cold sample. Precooled HD gas is filled in the sample cell from the center and goes out from two ends to a vacuum chamber pumped by a turbo pump. The pump outlet is connected to the sample source chamber to circulate the HD gas sample. To insulate the optical cavity from the mechanical noise generated by the cooler, we separate the ring-down cavity mirrors with the sample cell and damp the vibration with several stage bellows. An external cavity diode laser (ECDL) operating at around 1380 nm delivers three beams. The first one is frequency shifted by around −160 MHz with an acousto-optical modulator (AOM), in a double-pass scheme, and locked to the optical cavity with the Pound-Drever-Hall (PDH) method. The second beam with most of the laser power is frequency shifted by +80 MHz and chopped by another AOM before entering the cavity for ring-down measurements. The driving frequencies of AOMs are precisely controlled to make both beams match respective cavity modes. The third beam is beating with an optical frequency comb (OFC), and a feedback signal is applied to

*These authors equally contributed to this work.
†cfcheng@ustc.edu.cn

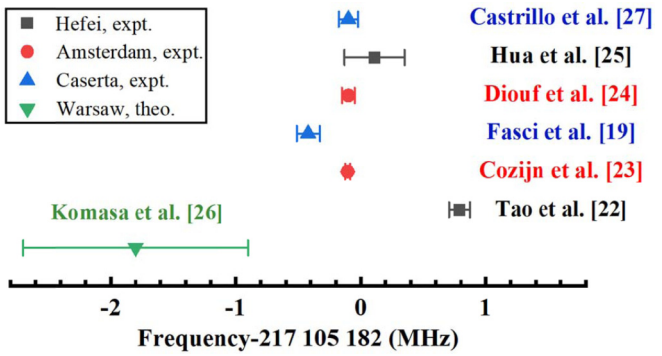

FIG. 1. Comparison of the HD R(1) (2-0) transition frequencies given in previous studies. The theoretical value [26] is marked as the green inverted triangle. The experimental results given by the Hefei [22,25], Amsterdam [23,24], and Caserta [19,27] groups are marked as black squares, red dots, and blue triangles, respectively.

the PZT to lock the laser frequency to the comb. Therefore the stabilized optical cavity provides short-term frequency stability to the laser and transfers the absolute accuracy of the frequency standard. A function generator is implemented to tune the beat frequency and consequently scan the laser. All the above-mentioned radio frequencies and the OFC are disciplined by a GPS-traced Rb clock with a long-term relative accuracy better than 10^{-12}.

The comb-locked CRDS technique was adopted here for the following reasons: (i) using a high-finesse cavity, CRDS allows a sensitivity at the level of 10^{-13}cm^{-1}, (ii) the laser power inside the cavity is enhanced to a few hundred Watts with a milli-Watt diode laser, and (iii) CRDS has no extra modulation-demodulation process, which avoids possible distortion of the line profile. Owing to the enhanced population at $J = 1$ level and reduced saturated absorption linewidth, the amplitude of the spectrum measured at 76 K would be about 10 times larger than that recorded at room temperature. Moreover, the interference due to nearby water absorption

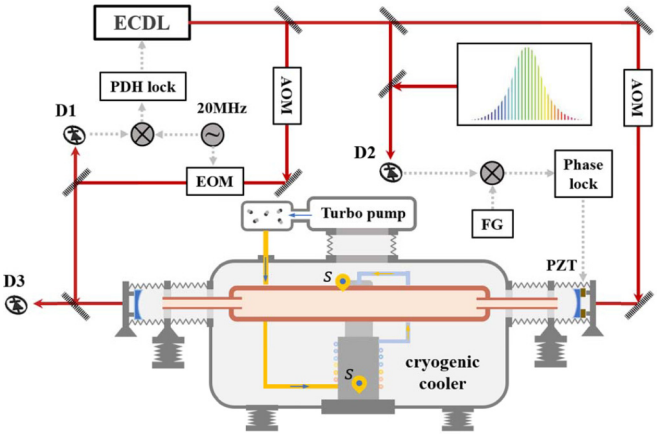

FIG. 2. The experimental apparatus. The red lines represent the laser beams, and the blue color indicates the ring-down cavity mirrors. AOM: Acousto-optical modulator; EOM: Electro-optical modulator; FG: Function generator; S: Temperature sensor; D1: Detector for PDH lock; D2: Detector for laser beating; D3: Detector for ring-down events.

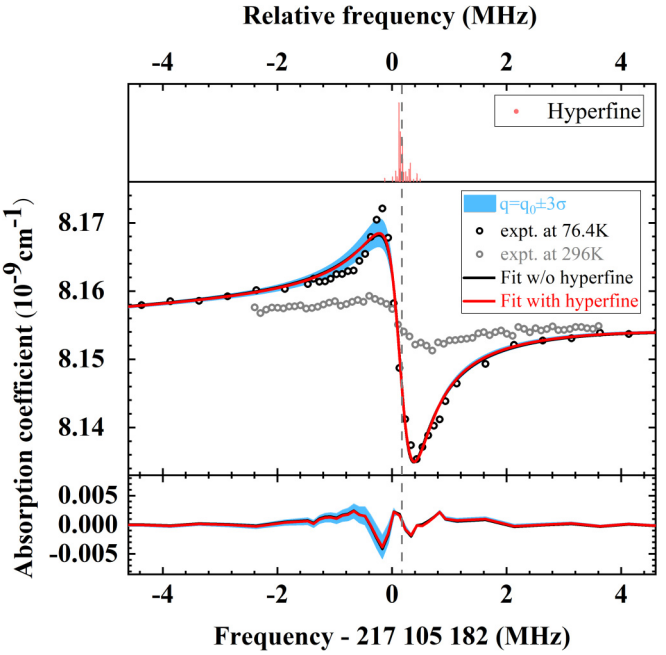

FIG. 3. Saturated absorption spectroscopy of the R(1) (2-0) line of HD. Black circles are experimental data recorded at 76 K. Gray circles are the room-temperature data taken from [25]. The red and black curves are the fitted line with and without hyperfine components, and their residuals are given in the lower panel. The gray dashed line indicates the fitted center. The blue belt indicates the simulated spectra with the Fano factor tuned between $q_0 + 3\sigma$ and $q_0 - 3\sigma$, where $q_0 = -0.721$ and $\sigma = 0.021$. In the upper panel, a stick spectrum of the hyperfine structure of this transition [26,28,29] is plotted with its center of gravity aligned to the vertical dash line.

lines is eliminated at such a low temperature since the water vapor pressure vanishes. In general, our setup provides an intracavity power of 250 W and equivalent absorption path length of about 80 km, which is sufficient for saturated absorption measurement of HD vibrational transition.

Results. The saturated absorption spectra of the R(1) line were measured at about 76 K, and an example spectrum is shown in Fig. 3. The noise equivalent absorption coefficient was about 1.7×10^{-13} cm^{-1} after averaging 3372 scans obtained in 40 h. Different from the conventional Lamb-dip spectrum, the measured spectral profile exhibits a significant asymmetric line shape, agreeing with our previous CRDS measurement at room temperature [25], and the spectrum observed at low temperature has a better signal-to-noise ratio. According to the strength of the HD line, the average density of HD molecules along the optical path was estimated to be 7×10^{14} molecules/cm^3 from the Doppler-broadened spectra.

The observed asymmetric spectra could be fit by the Fano profile [25,30,31]. Since the hyperfine structure was not resolved in this measurement, the same Fano factor q was used for all the hyperfine components in the fit:

$$\phi(\nu) = G(\nu - \nu_0) + D_{sat} \sum_i s_i \left(\frac{\left(2\frac{\nu-\nu_0-x_i}{\Gamma_0}+q\right)^2}{\left(2\frac{\nu-\nu_0-x_i}{\Gamma_0}\right)^2+1} - 1 \right), \quad (1)$$

where $G(\nu - \nu_0)$ is the Gaussian function describing the Doppler-broadened absorption background, ν and ν_0 are the

laser frequency and the transition center frequency, $D_{\rm sat}$ is depth of the saturated absorption, s_i and x_i are the relative intensity and frequency shift for each hyperfine component, respectively, and Γ_0 is the FWHM of the saturated absorption, which is dominated by the transit-time broadening. The Doppler profile is fixed according to calculated values under the experimental conditions, s_i and x_i values are fixed as those given in Ref. [26], and ν_0, q, Γ_0, and $D_{\rm sat}$ are free fitting parameters. The fitting result is shown in Fig. 3 (red curve). The Γ_0 value estimated with the fit is 539 (27) kHz, which is in fair agreement with the calculated transit-time broadening the value of 608 kHz [32]. The experimentally measured center frequency is 217 105 182 173 kHz with a statistical uncertainty of 11 kHz. Considering the correlation between the parameter q and ν_0, we also fit the spectrum with a varying q value within the range of $\pm 3\sigma$ ($\sigma = 0.021$) around $q_0 = -0.721$, and the results are shown as the blue belt in Fig. 3. We can see a considerable change in the fitting residuals, and the resulting change in ν_0 is ± 24.5 kHz, which could be a conservative estimation of the parameter decoupling uncertainty of the ν_0 value obtained from the fit. In addition, we also fit the spectrum using a single Fano function. The result is shown in Fig. 3 as the black curve, which overlaps with the red curve, and no considerable difference is found in resulting residuals and parameters.

As discussed in Ref. [31], the presence of a strong standing-wave field inside the cavity could couple with far off-resonance strong electronic transitions and induce a periodic modulation (amplitude of the modulation noted as δ) of the rotation-vibration energies through ac Stark shift, which eventually leads to a Fano-like line shape and a systematic shift to the measured line center. For the induced modulation amplitude of the transition due to the distant electronic states δ, its influence on the line center could be estimated by the numerical quantum optics calculations. The Fano factor q and the line center could be acquired through fitting the simulated absorption spectra based on the Floquet Hamiltonian:

$$H/\hbar = \sum_j \left\{ [\Delta_{12} + \delta \cos^2(k_p V_j t)]\sigma_{22}^j - \Omega_{12}\cos(k_p V_j t)\left(\sigma_{12}^j + \sigma_{21}^j\right)\right\}, \tag{2}$$

where superscript or subscript j indicates the jth molecule, $\Delta_{12}/2\pi = \nu - \nu_{12}$, ν is the frequency of the probe field, ν_{12} is the transition frequency of the two-level system, k_p is the wave vector of the laser, $\sigma_{ab} = |a\rangle\langle b|$, V_j is the longitudinal velocity for the jth molecule, and Ω_{12} is the Rabi frequency of the resonant coupling. Note that the initial position z_0 of the molecule is not shown in Eq. (2). Since the molecule moves through multiple periods of standing-wave length ($\lambda \approx 1.4\ \mu$m) in the longitudinal direction when it passes the laser beam (waist width $r = 0.45$ mm), the initial position z_0 of the molecule only determines the starting position of the first standing-wave period. The difference in the overall effect due to a different z_0 value could be negligible under our experimental conditions, since the molecule passes through dozens of standing-wave periods. For an ensemble of molecules, the susceptibility is contributed by the statistics of the nondiagonal density matrix elements of each molecule, where the imaginary and real parts correspond to the absorption and dispersion of the ensemble, respectively. Thus the mean excitation probability $\mathcal{P}$ to the near-resonant level is calculated as

$$\mathcal{P} = \frac{i}{2}\int_{-\infty}^{\infty} f(V)dV \int_0^{\infty} g(V_t)dV_t \int_0^{\frac{r}{V_t}} [\Omega_{12}(V,t') \times \rho_{21}(V,t') - \Omega_{12}^*(V,t')\rho_{12}(V,t')]dt', \tag{3}$$

which averages over the ensemble by considering different longitudinal velocities (V) and transverse velocities (V_t). According to the Maxwell-Boltzmann distribution of ideal gas, $f(V)$ and $g(V_t)$ as the one-dimensional and two-dimensional Maxwell-Boltzmann distribution functions, respectively, can be obtained. Here the density matrix elements ρ_{12}, ρ_{21} can be calculated by numerically solving the master equation [33] according to the Hamiltonian Eq. (2).

The hydrogen molecule has a number of electronic states which may contribute to the Fano-like line shape discussed above. For example, the ($B^1\Sigma_u^+$ - $X^1\Sigma_g^+$) transition has an Einstein coefficient at the level of 10^9 s^{-1}, which is stronger than the target infrared transition by 14 orders of magnitude. The contribution may mainly come from certain electronic states, but we could not identify which are the dominant states at the present stage. Either one-photon transitions to states such as $B^1\Sigma_u^+$ and $C^1\Pi_u$, or two-photon transitions to the $EF^1\Sigma_g^+$ state, and their rovibrational sublevels could contribute to the modulation of the target transition levels. For a conservative estimation of the effect, we consider only the transition from the upper level of the R(1) line ($v = 2, X^1\Sigma_g^+$) to the nearest electronic state $B^1\Sigma_u^+$. Using the transition rate, frequency, and Franck-Condon factors of the $B^1\Sigma_u^+$ - $X^1\Sigma_g^+$ transition given in Refs. [34–36] and the calculation method given in [31], we obtained a modulation amplitude of $\delta/2\pi = 0.08$ MHz on the target level. Taking the most probable transit time $\tau = 0.69\ \mu$s, our calculation shows that the interference due to this far off-resonance but very strong transition will induce an asymmetric Fano-like line shape in the saturated spectroscopy with a Fano factor of $q = -0.5$. It means that although the electronic transition frequency ($\sim$90 000 cm^{-1}) is extremely distant from the probing laser frequency (7200 cm^{-1}), the perturbation due to the electronic transition could be significant under our experimental conditions. Accurate δ and q values can be computed if more electronic states, including all the sublevels (vibration, rotation, and hyperfine structure), are taken into account in the calculation, which is beyond the scope of the present work.

Although the exact modulation amplitude δ is unknown, we could derive the systematic shift between the transition frequency and the Fano model fitted center by comparing the numerical results to the experimental result, as shown in Fig. 4(a). First we calculated saturated absorption spectra with various modulation amplitudes δ and transit times τ. Here, for a beam waist width of r, the transit time of the molecule is proportional to $\tau = r/V_t$, and we assume the molecules have a uniform distribution in the laser beam, resulting in an averaged temporal integration in Eq. (3). Then we derived the parameters q, Γ_0, and $\Delta\nu = \nu_0 - \nu_{12}$ by fitting the spectra, and the results are shown in Fig. 4(b). We can see that the absolute value of frequency shift $\Delta\nu$ increases with the absolute value of the Fano factor q, being consistent with

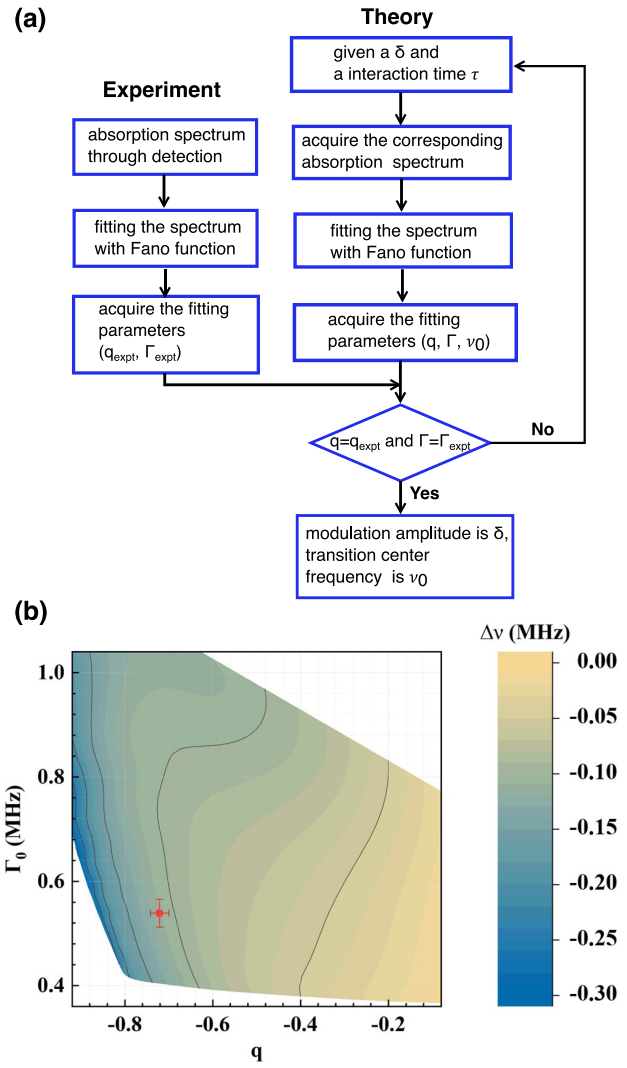

FIG. 4. (a) The logic diagram of the numerical calculation to acquire the transition center frequency ν_0. (b) The parameters (q, Γ_0, $\Delta\nu = \nu_0 - \nu_{12}$) acquired from numerical simulations of the asymmetric saturated absorption spectra, with the q being the corresponding fitting Fano factor for a set of given parameters with the modulation amplitude $\delta/2\pi$ in the range of 0.01–3.00 MHz. Other parameters of the model are fixed as $A_{12} = 2.148 \times 10^{-5}$ Hz, $T = 76$ K, intracavity optical power $P = 250$ W, $r = 0.45$ mm. The red dot indicates the experimental q and Γ_0 with their fitting errors.

the theory of Ref. [31]. The (q, Γ_0) value obtained from fitting the experimental spectrum is marked as the red dot in Fig. 4(b), corresponding to a frequency shift of −111.4 kHz. The frequency shift is in general proportional to the modulation amplitude δ and should be corrected for the transition center frequency. The uncertainty of the frequency shift is 12.3 kHz, including the error of 4.5 kHz from the calculation and a deviation of 11.4 kHz corresponding to the experimental uncertainties of q and Γ_0 [red error bars shown in Fig. 4(b)].

Other contributions to the uncertainty budget are discussed as follows. The recoil effect induces a doublet with a splitting of 68 kHz for the R(1) (2-0) line of HD, but no frequency shift needs to be considered. No collision-induced frequency shift is observed in current accuracy, agreeing with the previous study [25]. We carried out simulations at magnetic fields of 0.5 and 1 G, and no frequency shift could be observed. Other effects were investigated and are negligible in the experiment, including the comb frequency, the locking servo stability, and the AOM frequency drift. The second-order Doppler shift is +0.5 kHz with uncertainty of about 0.01 kHz. Finally, we determine the frequency for the HD R(1) (2-0) transition as 217 105 182 284 $(11)_{\rm stat}$ $(27)_{\rm sys}$ kHz. The systematic uncertainty is mainly from the correlation among parameters (24.5 kHz) and the line-shape model (12.3 kHz).

We also measured the transition with an intracavity laser power of 121 W and obtained the center frequency of 217 105 182 205 $(14)_{\rm stat}$ kHz, and the uncertainty of correlation among parameters is ±30.4 kHz. The calculated frequency shift is -68.4 ± 8.7 kHz through the same calculation method given above to obtain the estimation of the frequency shift. Taking into account the frequency correction, we determine the transition frequency of the HD R(1) (2-0) as 217 105 182 273 $(14)_{\rm stat}$ $(32)_{\rm sys}$ kHz. It agrees well with the value 217 105 182 284 $(11)_{\rm stat}$ $(27)_{\rm sys}$ kHz obtained with the intracavity laser power of 250 W.

Discussion. Saturated absorption spectroscopy of HD at a temperature as low as 76 K shows an extraordinary asymmetric line shape. The spectrum can be fitted with the Fano function and analyzed by solving the Floquet Hamiltonian. Our result is in agreement with the previous experimental result [25] measured at room temperature and improves the accuracy by a factor of 9. The improvement mainly comes from two aspects: one is that the measurement at lower temperature increases the experimental signal-to-noise ratio, and the other one is the clarified line-shape model reduces the ambiguity in the spectral fitting. Moreover, neither wavelength nor cavity modulation was applied in the present experiment, while the profile could be sensitive to the modulation phase in wavelength-modulated measurements [24,25]. Amsterdam's recent result [24] deviates from this work by −384(58) kHz, or 6.6 times the standard deviation, where a different treatment of the asymmetric line shape was applied. Note that Tao (2018) [22] and Cozijn (2018) [23] values were derived by fitting the spectra with symmetric Lorentzian profiles. As for Hua's result [25], the frequency shift induced by the asymmetric line shape has not been considered. According to the theory in Ref. [31], the modulation amplitude δ depends only on the molecular energy levels and the intracavity laser power. Using the δ value derived from this work that HD probed by an intracavity optical power of 250 W at low temperature, we can estimate the δ value in Hua's experiment at room temperature. With that estimated δ value, the corresponding spectrum can be simulated and parameters q, Γ, $\Delta\nu$ are −0.85, 777 kHz, and −84.5 kHz, acquired from fitting with the Fano function. Such a q value is consistent with the result obtained by Hua *et al.*, which was given as −0.94(2). Although accurate δ and q values are not fully computed in this work, we derive the transition frequency and its uncertainty in the framework of the present model.

The deviation between the calculated frequency value of R(1) in the (2-0) band and this work is $-2.1 \pm (0.9)_{\rm calc} \pm (0.03)_{exp}$ MHz [26]. As a comparison, the discrepancy for the R(0) line in the (1-0) band is $-1.0 \pm (0.6)_{\rm calc} \pm (0.013)_{exp}$ MHz [20,26], and that for the dissociation energy is

$-35 \pm (0.8)_{\mathrm{calc}} \pm (11)_{exp}$ MHz [4,37]. It indicates a possible systematic deviation between the theory and experiments in the HD molecule, which is proportional to the energy interval. It is expected that further improvements in both experimental and calculated spectroscopy of HD will allow an independent determination of the proton-to-electron mass ratio with a fractional uncertainty at the level of 10^{-11}, which could be compared with those obtained from the spectroscopy of HD^+ [38–41] and the Penning trap measurement [42,43].

Acknowledgments. This work was jointly supported by the Strategic Priority Research Program of the Chinese Academy of Sciences (Grants No. XDB21020100 and No. XDC07010000), and by the National Natural Science Foundation of China (Grants No. 11974328, No.11874342, No. 21688102, and No. 11922411). Numerical calculations in this work were partially done on the supercomputing system in the Supercomputing Center of the University of Science and Technology of China.

[1] K. Pachucki and J. Komasa, J. Chem. Phys. **130**, 164113 (2009).
[2] J. Komasa, K. Piszczatowski, G. Łach, M. Przybytek, B. Jeziorski, and K. Pachucki, J. Chem. Theory Comput. **7**, 3105 (2011).
[3] M. Puchalski, J. Komasa, P. Czachorowski, and K. Pachucki, Phys. Rev. Lett. **122**, 103003 (2019).
[4] M. Puchalski, J. Komasa, A. Spyszkiewicz, and K. Pachucki, Phys. Rev. A **100**, 020503(R) (2019).
[5] R. K. Altmann, L. S. Dreissen, E. J. Salumbides, W. Ubachs, and K. S. E. Eikema, Phys. Rev. Lett. **120**, 043204 (2018).
[6] C.-F. Cheng, J. Hussels, M. Niu, H. L. Bethlem, K. S. E. Eikema, E. J. Salumbides, W. Ubachs, M. Beyer, N. Hölsch, J. A. Agner, F. Merkt, L.-G. Tao, S.-M. Hu, and Ch. Jungen, Phys. Rev. Lett. **121**, 013001 (2018).
[7] N. Hölsch, M. Beyer, E. J. Salumbides, K. S. E. Eikema, W. Ubachs, Ch. Jungen, and F. Merkt, Phys. Rev. Lett. **122**, 103002 (2019).
[8] J. Hussels, N. Hölsch, C.-F. Cheng, E. J. Salumbides, H. L. Bethlem, K. S. E. Eikema, Ch. Jungen, M. Beyer, F. Merkt, and W. Ubachs, Phys. Rev. A **105**, 022820 (2022).
[9] T. M. Trivikram, M. Schlösser, W. Ubachs, and E. J. Salumbides, Phys. Rev. Lett. **120**, 163002 (2018).
[10] K.-F. Lai, P. Czachorowski, M. Schlösser, M. Puchalski, J. Komasa, K. Pachucki, W. Ubachs, and E. J. Salumbides, Phys. Rev. Res. **1**, 033124 (2019).
[11] K.-F. Lai, V. Hermann, T. M. Trivikram, M. Diouf, M. Schlösser, W. Ubachs, and E. J. Salumbides, Phys. Chem. Chem. Phys. **22**, 8973 (2020).
[12] M. Beyer, N. Hölsch, J. Hussels, C.-F. Cheng, E. J. Salumbides, K. S. E. Eikema, W. Ubachs, Ch. Jungen, and F. Merkt, Phys. Rev. Lett. **123**, 163002 (2019).
[13] C.-F. Cheng, Y. R. Sun, H. Pan, J. Wang, A.-W. Liu, A. Campargue, and S.-M. Hu, Phys. Rev. A **85**, 024501 (2012).
[14] Y. Tan, J. Wang, C.-F. Cheng, X.-Q. Zhao, A.-W. Liu, and S.-M. Hu, J. Mol. Spectrosc. **300**, 60 (2014).
[15] D. Mondelain, S. Kassi, T. Sala, D. Romanini, D. Gatti, and A. Campargue, J. Mol. Spectrosc. **326**, 5 (2016).
[16] P. Wcisło, F. Thibault, M. Zaborowski, S. Wójtewicz, A. Cygan, G. Kowzan, P. Maslowski, J. Komasa, M. Puchalski, K. Pachucki, R. Ciurylo, and D. Lisak, J. Quant. Spectrosc. Radiat. Transfer **213**, 41 (2018).
[17] S. Kassi and A. Campargue, J. Mol. Spectrosc. **267**, 36 (2011).
[18] S. Vasilchenko, D. Mondelain, S. Kassi, P. Cermák, B. Chomet, A. Garnache, S. Denet, V. Lecocq, and A. Campargue, J. Mol. Spectrosc. **326**, 9 (2016).
[19] E. Fasci, A. Castrillo, H. Dinesan, S. Gravina, L. Moretti, and L. Gianfrani, Phys. Rev. A **98**, 022516 (2018).
[20] A. Fast and S. A. Meek, Phys. Rev. Lett. **125**, 023001 (2020).
[21] J. Komasa, M. Puchalski, P. Czachorowski, G. Łach, and K. Pachuck, Phys. Rev. A **100**, 032519 (2019).
[22] L.-G. Tao, A.-W. Liu, K. Pachucki, J. Komasa, Y. R. Sun, J. Wang, and S.-M. Hu, Phys. Rev. Lett. **120**, 153001 (2018).
[23] F. M. J. Cozijn, P. Dupré, E. J. Salumbides, K. S. E. Eikema, and W. Ubachs, Phys. Rev. Lett. **120**, 153002 (2018).
[24] M. L. Diouf, F. M. J. Cozijn, B. Darquié, E. J. Salumbides, and W. Ubachs, Opt. Lett. **44**, 4733 (2019).
[25] T.-P. Hua, Y. R. Sun, and S.-M. Hu, Opt. Lett. **45**, 4863 (2020).
[26] J. Komasa, M. Puchalski, and K. Pachucki, Phys. Rev. A **102**, 012814 (2020).
[27] A. Castrillo, E. Fasci, and L. Gianfrani, Phys. Rev. A **103**, 022828 (2021).
[28] P. Dupré, Phys. Rev. A **101**, 022504 (2020).
[29] H. Jóźwiak, H. Cybulski, and P. Wcisło, J. Quant. Spectrosc. Radiat. Transfer **253**, 107186 (2020).
[30] U. Fano, Phys. Rev. **124**, 1866 (1961).
[31] Y.-N. Lv, A.-W. Liu, Y. Tan, C.-L. Hu, T.-P. Hua, X.-B. Zou, Y. R. Sun, C.-L. Zou, G.-C. Guo, and S.-M. Hu, Phys. Rev. Lett. **129**, 163201 (2022).
[32] W. Demtröder, *Laser Spectroscopy 1: Basic Principles* (Springer, Berlin, 2014).
[33] H.-P. Breuer and F. Petruccione, *The Theory of Open Quantum Systems* (Oxford University Press, Oxford, England, 2002), p. 122.
[34] U. Hollenstein, E. Reinhold, C. A. de Lange, and W. Ubachs, J. Phys. B **39**, L195 (2006).
[35] U. Fantz and D. Wünderlich, At. Data Nucl. Data Tables **92**, 853 (2006).
[36] H. Abgrall and E. Roueff, Astron. Astrophys. **445**, 361 (2006).
[37] D. Sprecher, J. Liu, Ch. Jungen, W. Ubachs, and F. Merkt, J. Chem. Phys. **133**, 111102 (2010).
[38] S. Patra, M. Germann, J.-P. Karr, M. Haidar, L. Hilico, V. I. Korobov, F. M. J. Cozijn, K. S. E. Eikema, W. Ubachs, and J. C. J. Koelemeij, Science **369**, 1238 (2020).
[39] S. Alighanbari, G. S. Giri, F. L. Constantin, V. I. Korobov, and S. Schiller, Nature (London) **581**, 152 (2020).
[40] D. J. Fink and E. G. Myers, Phys. Rev. Lett. **127**, 243001 (2021).
[41] F. Köhler, S. Sturm, A. Kracke, G. Werth, and K. Blaum, J. Phys. B **48**, 144032 (2015).
[42] F. Heiße, F. Köhler-Langes, S. Rau, J. Hou, S. Junck, A. Kracke, A. Mooser, W. Quint, S. Ulmer, G. Werth, K. Blaum, and S. Sturm, Phys. Rev. Lett. **119**, 033001 (2017).
[43] S. Rau, F. Heiße, F. Köhler-Langes, S. Sasidharan, R. Haas, D. Renisch, C. Düllmann, W. Quint, S. Sturm, and K. Blaum, Nature (London) **585**, 43 (2020).